Astron. Astrophys. 338, 977–987 (1998)

ASTRONOMY AND ASTROPHYSICS

New Young Stellar Object candidates in the Chamaeleon I molecular cloud discovered by DENIS⋆

L. Cambrésy[1], **E. Copet**[1], **N. Epchtein**[2], **B. de Batz**[1], **J. Borsenberger**[3], **P. Fouqué**[1,5], **S. Kimeswenger**[4], **and D. Tiphène**[1]

[1] Observatoire de Paris, F-92195 Meudon Cedex, France
[2] Observatoire de la Côte d'Azur, BP 4229, F-06304 Nice Cedex, France
[3] Institut d'Astrophysique de Paris, 98 bis Bd. Arago F-75014 Paris, France
[4] Institut für Astronomie der Leopold-Franzens-Universität Innsbruck, Technikerstrasse 25, A-6020 Innsbruck, Austria
[5] European Southern Observatory, La Silla, Chile

Received 19 January 1998 / Accepted 22 June 1998

Abstract. We present an analysis of point sources discovered by DENIS in an area of $\approx 1\overset{\circ}{.}5 \times 3\overset{\circ}{.}$ around the Chamaeleon I molecular cloud. Most of the $30\,000$ objects detected in the J band are background stars that were previously used to derive an accurate extinction map of the full area (Cambrésy et al., 1997) using star counts. Here, we investigate the young stellar population of the cloud using the $IJK_{\rm s}$ photometric DENIS data. The whole sample of 126 already known YSOs, which are mainly T Tauri stars, are identified in the DENIS catalogue. Besides, we propose 54 sources as new candidates of YSOs. These new faint objects are selected according to their extremely red near infrared colour, that cannot be explained only by the reddening of the cloud. Moreover they are concentrated near the most obscured areas of the cloud. Pending spectroscopic measurements, the sources are interpreted as probable classical T Tauri stars that have escaped previous spectroscopic, IRAS or X-ray observations and pertaining to the low-end of the luminosity function. Assuming that they are reliable YSOs with massive accretion disks, and using theoretical pre-main-sequence tracks we estimate the age of this sample to be ranging from $5\,10^5$ to $4\,10^6$ years, an elapse of time that spans the range between the end of the star formation in the cloud and the maximum life time of the circumstellar disk.

Key words: stars: formation – stars: pre-main sequence – ISM: clouds – ISM: individual objects: Chamaeleon I

1. Introduction

The Chamaeleon Molecular Cloud is one of the most interesting targets to investigate the formation of low mass stars and the low mass end of the initial mass function (IMF), because of its nearby location and its position far away of the galactic plane ($b \approx -17°$) where the density of background stars is relatively small. A complete census of young objects requires to survey deeply wide areas in a spectral range that is not much hampered by dust extinction, namely the near and mid–infrared. This has been made possible only recently thanks to the release of data provided by large scale sky surveys in the near–infrared such as DENIS (Epchtein, 1997).

Low mass young stellar objects (YSOs) are characterised by Hα line emission (Hartigan, 1993) and an infrared excess that reveals the presence of circumstellar material in the near-infrared (Whittet et al., 1987; Whittet et al., 1991), or in the mid and far-infrared as shown by the IRAS (Rydgren, 1980; Baud et al., 1984; Assendorp et al., 1990; Prusti et al., 1991) and ISO (Nordh et al., 1996) data. X-ray emission surveys provided by the Einstein and ROSAT missions, have also contributed to identifying young objects (Lawson et al., 1996; Alcalá et al., 1997). Finally, millimetre observations (Mattila et al., 1989; Henning et al., 1993), mostly in CO lines, allow the identification through the measurement of the gas emission and outflows that often characterise YSOs.

Known pre-main-sequence stars in the Chamaeleon cloud consist essentially of T Tauri stars (TTS) (Appenzeller & Mundt, 1989) of spectral type ranging from K5 to M5 (Appenzeller et al., 1983). Their mass ranges from 0.2 to $2M_\odot$ with a distribution peaking at $0.5M_\odot$, and their current age estimate is greater than 10^6 years, according to Lawson et al. (1996).

The Chamaeleon I (Cha I) cloud has been surveyed in various spectral ranges from millimetre to X-ray, but investigation are yet limited to small areas or low sensitivity.

During its first year of operations, DENIS has covered the whole surface of the Cha I cloud in the $IJK_{\rm s}$ bands with a good sensitivity ($K_{\rm s} < 13.5$). Thanks to its wide surface coverage, stars far away from the known cores of the cloud can be detected. An extinction map of the cloud was recently drawn out using J star counts (Cambrésy et al., 1997), and the aim of the present work is to pursue the exploitation of these data in order to pick up already catalogued TTS and to provide an homogeneous set

Send offprint requests to: Laurent Cambrésy, (Laurent.Cambresy@obspm.fr)

⋆ Based on observations collected at the European Southern Observatory, La Silla, Chile

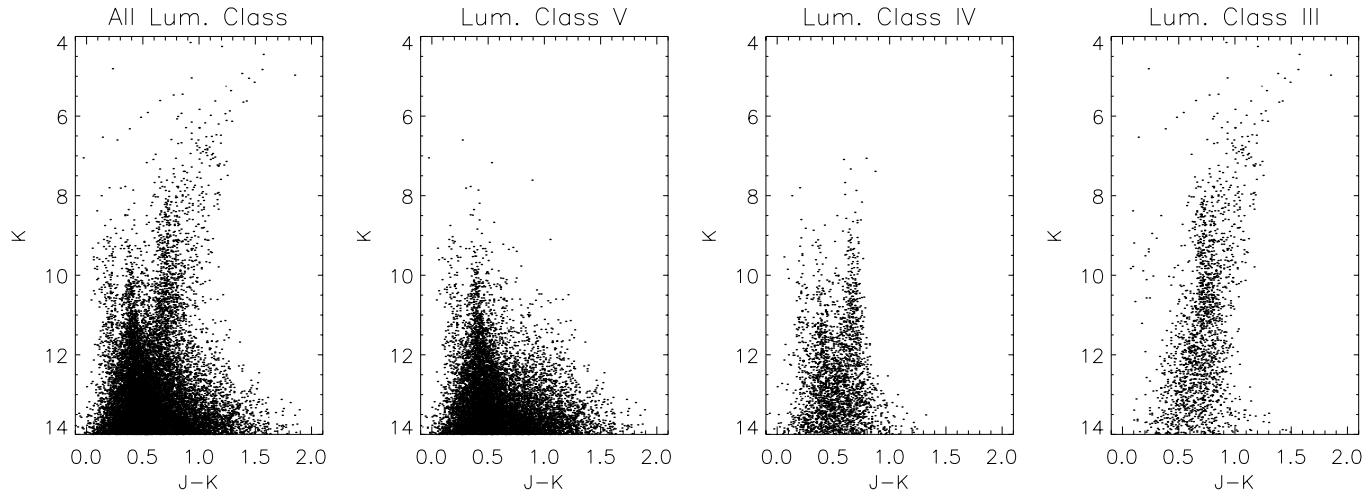

Fig. 1. Colour-magnitude diagram obtained with the *Besançon* model for the direction of the Chamaeleon I cloud (left), for different luminosity classes (others)

of data and to try to single out new YSO candidates, especially toward the low luminosity end.

Up to now, 126 pre-main-sequence stars have been recognised in the Cha I cloud by various authors. Sect. 2 presents the DENIS photometric data of these 126 stars and of 54 new candidates that have been selected using the method described in Sect. 3. The nature of the sources is discussed in Sect. 4.1 and some constraints on the circumstellar environments are derived in Sect. 4.2. Finally, in Sect. 4.3, we discuss the luminosity function, and we estimate the age of the period of star formation in the cloud.

2. Observations and results

The observations presented here have been collected as part of the DENIS survey between January and May 1996 at La Silla (Chile) using the ESO 1 metre telescope equipped with the specially designed 3-channel camera (Epchtein, 1997; Copet et al., 1998). They cover an area of $1.^{\circ}45 \times 2.^{\circ}94$ centred at $\alpha = 11^{\rm h}06^{\rm m}$, $\delta = -77^{\circ}30^{\rm m}$ (J2000) in three bands, namely I (0.8 μm), J (1.25 μm) and $K_{\rm s}$ (2.15 μm). They consist of 13 strips each involving 180 images of $12' \times 12'$ taken at constant RA along an arc of 30° in declination. The overlap between two adjacent strips reaches 75% in the Cha I cloud because of the proximity of the south pole. Wherever a star is picked up in two adjacent strips, position and flux values are averaged. Limiting magnitudes are 18, 16 and 13.5 at 3σ in I, J and $K_{\rm s}$ bands, respectively, and a conservative estimate of the position accuracy is $1''$ *rms* in both directions. The numbers of stars detected in $IJK_{\rm s}$ are $\sim$ 50 000, 30 000 and 10 000, respectively. Table 1 displays a list of known stars associated with the Cha I cloud with the DENIS positions and $IJK_{\rm s}$ photometry. Names given in column 4 refer to previous investigations quoted in the footnote 1 of the table. Column 9 lists the cloud extinction as measured on our map (Cambrésy et al., 1997), and col. 10 the extinction derived from the $I - J$ colour excess. Table 2 presents the list of our new candidates, their DENIS positions and photometry, and the extinction derived in the same way as in Table 1.

3. Selection method

3.1. Description

Our selection method of new YSO candidates is essentially based on the IR colours and magnitudes of the objects after de–reddening. However, before attempting to select new YSO candidates, we have first estimated the contamination by background and foreground stars and the influence of the luminosity classes on the star magnitudes. To derive this information, we have run the so called *Besançon* model (Robin & Crézé, 1986) in the direction of the Cha I cloud. The model has been parametrised to take into account the DENIS limiting magnitudes and photometric errors. It neglects the cloud itself (extinction, star formation). Fig. 1 displays synthetic colour-magnitude diagrams obtained for the different classes of luminosity using this model. The brightest stars ($K_{\rm s} < 8$) correspond to highly red giants ($J - K_{\rm s} > 1$), and the colour dispersion of the faintest stars results of the photometric errors. We must keep in mind these two points before using an infrared excess criterion to identify the YSOs. It is clear that we can identify only the objects exhibiting a strong infrared excess, i.e $J - K_{\rm s} > 1$. The number of objects detected both in J and $K_{\rm s}$ band within the covered area is $\sim$ 10 000, while the model yields only some 150 foreground stars, i.e. less than 2%, assuming a distance of the cloud of 140 pc.

A previous investigation based on DENIS star counts in the J band on the Cha I cloud enabled us to draw an accurate extinction map (Cambrésy et al., 1997) with a spatial resolution of $2'$. The peak of visual absorption that was measured is about 10 magnitudes. This map is used to deredden all the stars detected within the area that it encompasses. For those stars located inside the cloud, this reddening is, of course, an upper limit.

Table 1. List of known T Tauri stars

Nb	R.A. (J2000)	Dec. (J2000)	Name[1]	V	I	J	K_s	Av_{cl}	Av_*
(1)	(2)	(3)	(4)	(5)	(6)	(7)	(8)	(9)	(10)
1[2]	10 52 03.0	-77 09 49	T1, Sz1						
2[3]	10 54 30.0	-77 55 18	T2, SW Cha					0.0	
3[4]	10 56 01.1	-77 24 38	T3, SX Cha	14.65		10.20	8.38	0.9	
4[5]	10 56 32.0	-77 11 38	T4, SY Cha	13.03		10.09	8.74	2.7	
5	10 57 42.7	-76 59 36	T5, Sz4		12.18	10.31	9.04	1.2	3.3
6	10 58 05.9	-77 28 24	CHRX3	12.26	9.99	8.33	7.04	1.4	2.6
7	10 58 17.1	-77 17 17	T6, SZ Cha	11.99	10.32	8.96	7.43	1.0	1.7
8	10 59 01.4	-77 22 41	T7, TW Cha	13.08	11.26	9.87	8.18	1.4	1.8
9	10 59 07.5	-77 01 40	T8, Sz6, CHX3	11.22	9.82	8.40	7.16	0.9	1.9
10	11 00 14.5	-76 44 15	T9, Sz7		12.22	8.96	7.38	0.5	7.4
11	11 00 14.9	-77 14 38	CHXR8	11.45	10.49	9.85	9.45	1.4	0.0
12	11 00 40.7	-76 19 28	T10, Sz8		13.47	11.82	10.69	0.1	2.5
13	11 01 19.0	-76 27 03	CHXR9C	14.11	11.60	10.04	8.81	0.5	2.3
14	11 02 15.4	-77 10 59	B9		14.80	13.51	12.62	0.2	1.5
15	11 02 25.4	-77 33 36	T11, CS Cha	11.63	10.12	9.00	8.26	5.0	1.0
16	11 02 33.0	-77 29 13	Hn1		12.97	11.23	10.16	4.3	3.0
17	11 02 55.5	-77 21 51	T12, Sz10		13.14	11.41	10.36	1.4	3.0
18	11 03 12.0	-77 21 05	CHXR11	11.52	9.58	8.11	7.15	1.3	2.0
19	11 03 48.1	-77 19 57	Hn2		13.91	11.26	9.96	1.4	5.5
20[6]	11 03 51.4	-76 55 46	T13, TZ Cha		15.04	14.35		0.1	0.0
21	11 03 57.3	-77 21 34	Hn3		12.51	10.75	9.69	1.9	2.9
22	11 04 09.5	-76 27 19	T14, CT Cha	12.36	10.89	9.63	8.54	0.1	1.4
23	11 04 11.6	-76 54 32	CHXR72	15.04	13.09	11.79	10.96	0.0	1.2
24	11 04 23.2	-77 18 08	T14a, HH48		16.25	14.48	12.36	2.2	2.9
25	11 04 24.7	-77 25 49	T15, Sz12		13.35	10.87	9.45	3.8	5.0
26	11 04 43.0	-77 41 57	B18		13.63	11.78	10.61	6.1	3.1
27	11 04 51.5	-76 25 24	CHXR14N	14.13	11.89	10.59	9.61	0.5	1.5
28	11 04 53.2	-76 25 51	CHXR14S	14.66	12.05	10.67	9.64	0.5	1.7
29	11 04 57.4	-77 15 57	T16, Sz13		14.80	12.10	10.27	2.9	5.7
30	11 05 15.1	-77 11 29	Hn4		13.38	10.93	9.46	2.8	4.9
31	11 05 15.6	-77 52 55	T18, Sz14		15.54	13.01	11.25	4.4	5.2
32	11 05 22.0	-76 30 22	T17, UU Cha		14.36	13.44	12.61	1.4	0.4
33	11 05 41.9	-77 54 44	T19, Sz15		12.35	11.29	10.64	4.3	0.8
34	11 05 43.4	-77 26 52	CHXR15	17.27	13.53	11.29	10.09	6.0	4.2
35	11 05 53.0	-76 18 26	T20, UV Cha	13.79	11.93	10.43	9.21	0.5	2.1
36	11 06 15.7	-77 21 57	T21, CHX7	11.28	9.42	7.66	6.27	6.2	2.9
37	11 06 42.3	-76 35 49	Hn5		14.15	11.88	10.14	2.4	4.2
38	11 06 43.9	-77 26 35	T22, UX Cha		13.02	10.94	9.27	5.8	4.0
39	11 06 45.5	-77 27 03	CHXR20	14.76	12.00	10.31	8.76	5.0	2.7
40	11 06 47.1	-77 22 31	Ced110 IRS4				12.95	6.9	
41	11 06 59.5	-77 18 54	T23, UY Cha		12.92	11.30	9.89	9.0	2.7
42	11 07 09.8	-77 23 05	Ced110 IRS6				10.94	7.1	
43	11 07 10.8	-77 43 44	CHXR22W		16.72	14.15	12.52	4.8	5.4
44	11 07 11.8	-77 46 39	Hn6		13.34	11.17	9.59	4.5	4.0
45	11 07 12.5	-76 32 23	T24, UZ Cha	14.90	12.49	10.86	9.23	2.8	2.4
46	11 07 13.7	-77 43 50	CHXR22E		14.84	11.93	9.96	4.8	6.3
47	11 07 19.6	-76 03 05	T25, Sz18	15.35	12.61	11.04	9.84	0.6	2.4
48	11 07 21.1	-77 38 08	T26, Sz19, CHX9	10.68	9.31	8.02	6.34	5.8	1.2
49	11 07 28.6	-76 52 12	T27, VV Cha	14.80	12.26	10.73	9.60	1.4	2.5
50	11 07 33.4	-77 28 28	CHXR25	15.99	13.14	11.78	10.88	5.5	1.7
51	11 07 35.7	-77 34 50	CHXR76		14.43	12.14	10.90	6.3	4.5
52	11 07 37.4	-77 33 34	CHXR26		15.16	11.56	9.31	6.2	8.4
53	11 07 44.1	-77 39 42	T28, Sz21	15.34	12.56	10.20	8.34	5.0	4.6
54	11 07 56.3	-77 27 26	CHX10a, F29		11.01	9.12	7.80	5.4	3.2
55	11 07 57.7	-77 17 27	Baud38		17.42	13.08	9.87	6.5	10.6
56	11 07 58.4	-77 38 45	T29, Sz22	14.2	12.76	10.18	7.19	4.2	5.3
57	11 07 58.5	-77 42 42	T30, Sz23, CHX11		14.58	11.98	9.92	4.0	5.4
58	11 08 00.4	-77 17 31	CHXR30		15.57	11.74	9.04	7.4	9.1

Table 1. (continued)

Nb	R.A. (J2000)	Dec. (J2000)	Name[1]	V	I	J	K_s	Av_{cl}	Av_*
(1)	(2)	(3)	(4)	(5)	(6)	(7)	(8)	(9)	(10)
59	11 08 01.9	-77 42 29	T31, VW Cha	12.51	10.56	8.66	6.98	4.0	9.1
60	11 08 03.7	-77 39 18	T32, HD 97048	8.45	8.58	7.39	6.26	4.2	0.7
61	11 08 15.8	-77 33 54	T33, CHX12		10.54	8.58	6.22	5.4	3.3
62	11 08 17.0	-77 44 37	T34, Sz26		13.04	11.03	10.05	4.0	3.6
63	11 08 37.1	-77 43 51	IRN		15.86	11.93	8.48	3.9	9.4
64	11 08 39.5	-77 16 05	T35, Sz27	16.28	13.22	11.89	8.89	4.7	4.9
65	11 08 41.1	-76 36 08	CHX13a	15.56	12.54	10.45	9.09	3.3	3.2
66[7]	11 08 49.7	-76 44 28	T36, VX Cha					2.0	
67[8]	11 08 51.2	-77 43 39	C9-1					3.6	
68	11 08 51.3	-76 25 14	T37, Sz28		14.74	12.45	11.30	1.1	4.3
69	11 08 54.7	-77 32 12	CHXR78C		14.75	12.17	10.92	4.0	4.9
70	11 08 55.1	-77 02 13	T38, VY Cha		12.99	11.12	9.26	2.3	3.0
71	11 09 05.5	-77 09 58	Hn7		13.83	11.79	10.77	2.6	3.5
72	11 09 12.3	-77 29 13	T39, Sz30, CHX14	13.17	11.22	9.72	8.75	3.9	1.8
73	11 09 14.2	-76 28 40	Hn8		13.69	11.64	10.67	2.3	3.4
74	11 09 18.1	-76 27 58	CHXR37	13.92	11.66	9.87	8.41	2.3	2.7
75	11 09 18.6	-76 30 29	Hn9		14.91	11.63	8.95	4.9	7.3
76	11 09 23.0	-76 34 32	C1-6		17.99	13.13	9.32	4.0	11.4
77	11 09 24.2	-76 23 21	T40, VZ Cha	12.75	11.43	9.82	7.71	0.8	2.4
78	11 09 40.5	-76 28 39	CHXR40	14.04	11.47	9.95	8.73	2.3	2.0
79	11 09 42.4	-76 34 58	C1-25			13.49	9.80	5.6	
80	11 09 43.0	-77 25 59	C7-1		15.71	12.19	10.42	5.1	7.8
81	11 09 46.2	-76 43 54	C2-3		14.50	11.75	9.96	2.9	5.7
82	11 09 46.6	-76 34 46	Hn10E		14.81	11.93	9.84	5.6	6.3
83[9]	11 09 46.6	-76 34 46	Hn10W					5.6	
84	11 09 47.8	-77 26 30	Baud43		16.02	12.38	9.93	4.5	7.9
85	11 09 50.4	-76 36 48	T41, HD 97300		8.84	7.56	7.05	4.1	1.4
86	11 09 53.8	-76 34 25	T42, Sz32		14.61	10.62	6.42	5.8	9.6
87	11 09 54.4	-76 29 25	T43, Sz33, CHX15		13.99	11.29	9.17	2.8	5.7
88	11 09 55.5	-76 32 41	C1-2			13.87	9.52	6.1	
89	11 09 59.7	-77 37 09	T45, WX Cha	14.86	11.82	9.69	7.86	3.5	3.2
90	11 10 01.0	-76 34 58	T44, WW Cha	13.27	11.02	8.56	5.75	5.8	5.0
91	11 10 04.1	-76 33 29	Hn11		14.46	11.55	9.39	6.2	6.3
92	11 10 05.1	-76 35 45	T45a	14.34	11.93	10.23	9.04	5.4	2.7
93	11 10 07.4	-76 29 38	T46, WY Cha	13.98	11.60	9.87	8.31	2.8	2.8
94	11 10 28.9	-77 17 00	Hn12W		13.85	11.60	10.64	5.4	4.3
95[10]	11 10 28.9	-77 17 00	Hn12E					5.4	
96	11 10 38.4	-77 32 40	CHXR47, F34	14.42	11.66	9.59	8.23	2.8	3.8
97	11 10 50.0	-77 17 53	T47, Sz37	15.54	13.01	10.91	9.07	5.0	3.8
98	11 10 53.7	-76 34 32	T48, WZ Cha	15.26	12.76	11.08	9.95	3.5	2.6
99	11 10 56.4	-76 45 33	Hn13		13.85	11.13	9.96	4.2	5.8
100	11 11 14.6	-76 41 11	Hn14		16.25	14.17	12.70	3.4	3.8
101	11 11 35.2	-76 36 21	CHXR48	14.73	12.35	10.79	9.65	2.0	2.3
102	11 11 40.1	-76 20 15	T49, XX Cha	15.28	12.56	10.68	9.24	0.2	3.2
103	11 11 46.8	-76 20 09	CHX18N	12.05	10.37	9.02	7.75	0.4	1.6
104	11 11 54.5	-76 19 31	Hn15	14.41	11.88	10.14	9.12	0.4	2.8
105	11 12 03.7	-76 37 03	Hn16		13.97	11.69	10.66	1.8	4.4
106	11 12 10.3	-76 34 37	T50, Sz40		13.41	11.20	9.92	0.7	4.2
107	11 12 24.8	-76 37 06	T51, Sz41, CHX20	11.60	10.22	9.15	7.90	1.0	0.8
108	11 12 28.1	-76 44 22	T52, CV Cha	10.96	9.53	8.22	6.75	2.2	1.2
109	11 12 28.2	-76 25 29	CHXR53	14.72	12.19	10.81	9.86	0.5	1.7
110	11 12 31.4	-76 44 24	T53, CW Cha	14.45	13.50	11.22	9.22	1.5	4.4
111	11 12 42.6	-76 58 40	CHX21a		11.56	10.39	9.35	2.1	1.1
112	11 12 43.1	-77 22 23	T54, CHX22	11.16	9.64	8.58	7.71	2.3	0.8
113	11 12 43.4	-76 37 05	CHX20E		10.95	10.01	9.08	0.6	0.4
114	11 12 49.1	-76 47 07	Hn17		13.66	12.07	11.01	2.1	2.4
115	11 13 20.6	-77 01 04	CHXR57	14.63	12.27	10.87	9.79	0.8	1.8
116	11 13 24.9	-76 29 23	Hn18		13.51	11.78	10.64	0.2	2.7

Table 1. (continued)

Nb	R.A. (J2000)	Dec. (J2000)	Name[1]	V	I	J	K_s	Av_{cl}	Av_*
(1)	(2)	(3)	(4)	(5)	(6)	(7)	(8)	(9)	(10)
117	11 13 27.8	-76 34 17	CHXR59	14.35	12.09	10.54	9.55	0.1	2.4
118	11 13 30.1	-76 29 01	Hn19		13.40	11.53	10.45	0.1	3.0
119	11 13 34.0	-76 35 37	T55, Sz44		13.48	11.69	10.71	0.1	3.0
120	11 14 16.1	-76 27 37	Hn20		13.21	11.29	10.00	0.0	3.4
121	11 14 24.9	-77 33 07	Hn21W		14.36	12.04	10.57	1.6	3.3
122	11 14 26.6	-77 33 05	Hn21E		16.19	12.91	11.69	1.6	7.3
123	11 14 50.8	-77 33 39	B53		11.89	10.36	9.41	1.4	2.3
124	11 16 13.4	-77 14 07	CHXR65	13.33	11.88	10.87	10.16	0.0	0.6
125	11 17 37.4	-77 04 38	T56, Sz45	13.50	11.78	10.24	9.27	0.2	2.2
126	11 18 20.6	-76 21 58	CHXR68	13.37	10.96	9.69	8.72	0.0	1.4

[1] T# from Schwartz (1991) ; Sz# from Schwartz (1977) ; C# from Hyland et al. (1982), Jones et al. (1985) ; CHX# from Feigelson & Kriss (1989) ; CHXR# from Feigelson et al. (1993), Lawson et al. (1996) ; Baud# from Baud et al. (1984) ; Hn# from Hartigan (1993) ; B# from Alcalá PhD thesis, referenced in Lawson et al. (1996) ; Ced110 IRS# from Prusti et al. (1991)
[2] Out of field.
[3] Not detected in J nor in K_s, I not available.
[4] I not available.
[5] I not available.
[6] Not detected in K_s.
[7] Not detected by DENIS. Previous measurement (Prusti et al., 1992) have found $J = 13.60$ and $K = 12.77$. Since the detection limit is 16 in J this object should have important luminosity variation.
[8] Not detected by DENIS. Previous measurement (Hyland et al., 1982) have found $J = 13.84$ and $K = 10.66$. This object is in the line of sight of the Infrared Nebula (IRN).
[9] Not Detected. Measured by Hartigan (1993), $J = 18.10$ $K = 14.66$.
[10] Not Detected. Measured by Hartigan (1993), $J = 16.34$ $K = 14.58$.

The YSO candidates are selected according to their colour and magnitude properties after this dereddening has been applied. Consequently, we introduce a bias in the selection of the reddest objects that is discussed below.

In practice, we have plotted the dereddened magnitudes in a colour-magnitude diagram together with the main sequence (Fig. 2a and b) and selected the stars which are separated from the main sequence by a distance corresponding to 8 magnitudes of visual extinction, at least. This provides 90 stars. Part of them cannot be shifted towards the main sequence just assuming an even larger extinction, and are likely to be intrinsically very red. This sample, still contains some unreliable sources because of photometric errors and, also, some red giant background stars. After eliminating these objects which are, basically, the bright and the faint ends of the sample, we are left with the 54 good candidates listed in Table 2. All of them have been carefully checked afterwards by visual inspection of the DENIS images to avoid possible misleading cross-identifications between the 3 DENIS channels, or optical artifacts such as ghosts produced by nearby bright star or bad pixels.

3.2. Validity

Since the exact value of the extinction suffered by each star cannot be accurately determined, we have assumed that it is the total extinction measured on the line of sight and taken it as an upper limit. Consequently, the constraints on the star colours depend on the location of the star with respect to the cloud. The criterion is more strict for stars in the front edge of the cloud than for stars just behind the cloud. In other words, the infrared excess can be hidden by an overestimate of the reddening actually suffered by the stars. The stars that we possibly missed should be, in average, brighter than the selected stars because they are less obscured. Fortunately, the near–infrared range is less sensitive to extinction than optical bands. The average visual extinction in the Cha I cloud is about 4 magnitudes, i.e. $\lesssim 0.5$ magnitudes of K_s extinction. So, this effect does not introduce a significant bias in the luminosity function. We can crudely evaluate the maximum number of missed stars. Assuming that the extinction would be reduced by a factor 2, the total number of selected star with our infrared excess method would increase by a factor 1.7, i.e. ~ 37 additional stars. Most of them would probably be background stars because the extinction is now underestimated for these stars and thus, a residual infrared excess remains. Nevertheless, this provides an indication of the maximum number of stars that we can miss.

4. Discussion

4.1. Nature of the sources

In the final sample of 54 candidates, 34 are detected in the 3 channels, 16 only in J and K_s, and 4 only in K_s band (see Table 2). Fig. 2a and b displays a colour-magnitude and a colour-colour diagram for the known T Tauri Stars

Table 2. Position and DENIS colours of new YSO candidates

Nb	Id. name	R.A. (J2000)	Dec. (J2000)	I	J	K_s	Av_{cl}	Av_*
(1)	(2)	(3)	(4)	(5)	(6)	(7)	(8)	(9)
1	DENIS-P J1058.4-7826	10 58 22.9	-78 26 48	11.09	9.08	7.50	0.4	3.6
2	DENIS-P J1059.2-7826	10 59 12.3	-78 26 39	10.65	8.93	7.47	0.1	2.8
3	DENIS-P J1101.1-7730	11 01 03.2	-77 30 35		15.85	12.86	2.9	
4	DENIS-P J1101.5-7750	11 01 29.5	-77 50 41	17.39	16.10	13.14	4.2	1.5
5	DENIS-P J1101.5-7742	11 01 32.1	-77 42 10	13.57	10.73	8.68	3.8	6.1
6	DENIS-P J1102.4-7753	11 02 23.9	-77 53 23	16.78	13.14	10.88	5.0	8.5
7	DENIS-P J1102.4-7753	11 02 25.3	-77 53 15		15.86	12.95	5.0	
8	DENIS-P J1102.8-7738	11 02 47.1	-77 38 09		13.75	10.50	7.9	
9*	DENIS-P J1103.2-7736	11 03 11.5	-77 36 36		13.40	10.01	8.4	
10	DENIS-P J1103.5-7749	11 03 31.6	-77 49 02			12.77	9.4	
11	DENIS-P J1103.8-7747	11 03 45.7	-77 47 04			12.83	8.6	
12	DENIS-P J1104.2-7750	11 04 11.1	-77 50 13	18.48	13.88	10.64	9.0	11.4
13	DENIS-P J1105.0-7721	11 05 00.6	-77 21 47	16.26	14.28	12.84	3.8	3.5
14	DENIS-P J1105.3-7757	11 05 19.2	-77 57 39	18.13	13.74	10.34	6.8	10.8
15	DENIS-P J1105.3-7723	11 05 20.9	-77 23 02	16.85	14.00	12.16	4.7	6.2
16	DENIS-P J1105.4-7607	11 05 24.0	-76 07 44	11.99	10.00	8.41	0.4	3.6
17	DENIS-P J1105.9-7738	11 05 54.4	-77 38 43	15.52	11.52	8.90	6.3	9.6
18	DENIS-P J1105.9-7735	11 05 55.1	-77 35 13	17.98	13.19	9.75	6.4	12.0
19	DENIS-P J1106.3-7737	11 06 15.9	-77 37 51	16.55	12.72	10.08	6.5	9.1
20	DENIS-P J1106.3-7735	11 06 18.9	-77 35 18		16.21	12.93	6.7	
21*	DENIS-P J1107.2-7718	11 07 09.6	-77 18 47		15.12	11.32	9.9	
22	DENIS-P J1107.2-7646	11 07 10.1	-76 46 22	13.95	11.33	9.35	2.0	5.5
23	DENIS-P J1107.3-7723	11 07 16.8	-77 23 07			11.83	7.1	
24*	DENIS-P J1107.4-7722	11 07 21.9	-77 22 12		15.28	10.86	9.3	
25*	DENIS-P J1107.4-7741	11 07 24.4	-77 41 26	12.32	9.65	7.40	5.1	5.6
26	DENIS-P J1107.6-7735	11 07 37.2	-77 35 17	16.31	12.45	9.90	5.9	9.2
27	DENIS-P J1107.6-7733	11 07 37.8	-77 33 10	18.03	13.68	10.81	6.2	10.7
28	DENIS-P J1107.8-7738	11 07 45.6	-77 38 06	17.16	11.94	8.09	5.1	13.3
29	DENIS-P J1107.9-7743	11 07 55.7	-77 43 56	18.35	15.69	13.54	4.0	5.6
30	DENIS-P J1108.0-7737	11 07 58.2	-77 37 21		15.83	12.78	4.5	
31	DENIS-P J1108.0-7703	11 08 00.1	-77 03 54	17.82	16.02	11.88	1.3	3.0
32*	DENIS-P J1108.1-7738	11 08 03.4	-77 38 43	14.39	11.64	8.24	4.2	5.8
33	DENIS-P J1108.2-7718	11 08 12.0	-77 18 54		14.54	10.48	10.3	
34*	DENIS-P J1108.2-7719	11 08 12.9	-77 19 13		13.10	8.83	10.3	
35	DENIS-P J1108.9-7743	11 08 56.5	-77 43 30		15.10	12.40	3.8	
36	DENIS-P J1109.2-7632	11 09 11.0	-76 32 51		14.42	11.68	5.5	
37	DENIS-P J1109.2-7739	11 09 11.5	-77 39 06	16.14	12.70	10.29	5.1	7.9
38	DENIS-P J1109.4-7736	11 09 21.9	-77 36 54	16.74	13.93	12.00	4.0	6.0
39	DENIS-P J1109.4-7631	11 09 23.3	-76 31 14	18.20	14.34	11.70	5.0	9.2
40	DENIS-P J1109.4-7633	11 09 26.4	-76 33 34	17.77	13.14	10.11	6.3	11.5
41	DENIS-P J1109.5-7633	11 09 28.9	-76 33 28			12.24	6.3	
42	DENIS-P J1109.6-7710	11 09 38.1	-77 10 41	15.28	11.49	8.97	3.4	9.0
43	DENIS-P J1109.7-7633	11 09 43.5	-76 33 30		15.71	12.09	6.3	
44	DENIS-P J1109.8-7634	11 09 48.1	-76 34 06		15.17	11.83	5.6	
45	DENIS-P J1109.8-7714	11 09 49.2	-77 14 38		15.19	12.06	4.6	
46	DENIS-P J1109.9-7717	11 09 53.4	-77 17 15		15.16	12.20	5.9	
47	DENIS-P J1110.0-7718	11 09 57.1	-77 18 25	16.58	12.33	9.72	7.7	10.4
48*	DENIS-P J1110.2-7635	11 10 11.8	-76 35 29	13.90	10.77	8.51	4.1	7.0
49*	DENIS-P J1110.9-7725	11 10 54.0	-77 25 02	17.51	13.28	10.83	3.7	10.3
50	DENIS-P J1111.5-7609	11 11 29.5	-76 09 29	12.78	9.88	7.99	1.3	6.3
51*	DENIS-P J1111.5-7728	11 11 32.3	-77 28 11	14.90	11.63	9.43	3.8	7.4
52	DENIS-P J1113.0-7616	11 12 59.8	-76 16 53	11.93	10.09	8.56	0.2	3.1
53	DENIS-P J1114.2-7630	11 14 13.7	-76 30 54	16.47	15.30	12.91	0.0	1.1
54	DENIS-P J1114.3-7740	11 14 15.0	-77 40 57	16.63	15.04	12.34	1.3	2.4

* object detected by ISO in the LW2 and LW3 filter (P. Persi, private communication)

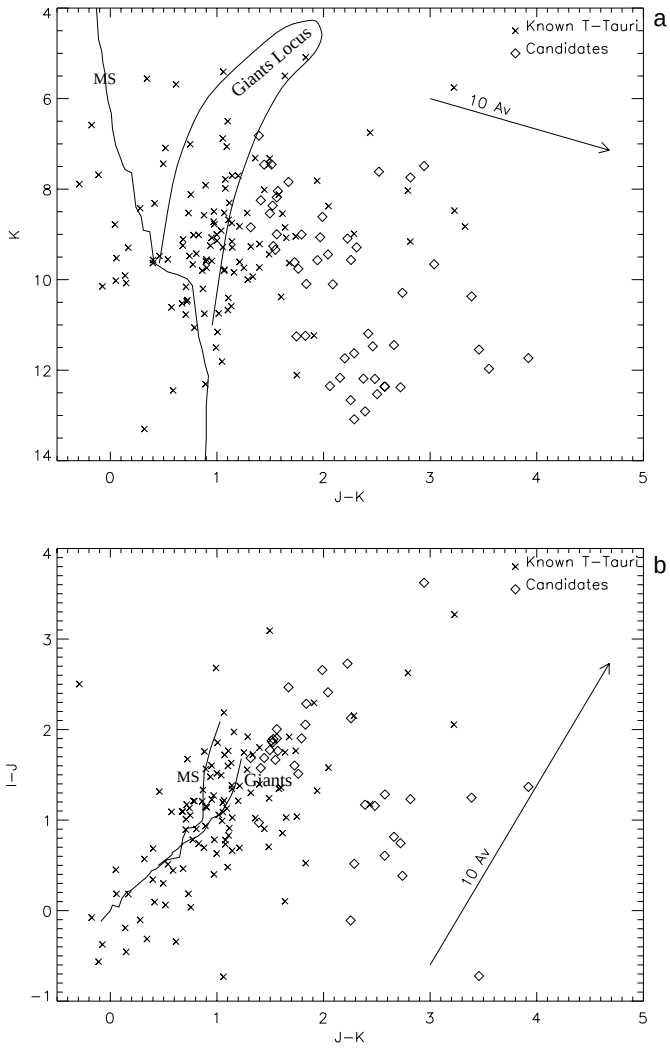

Fig. 2a and b. Dereddened diagram for known T Tauri stars and new DENIS selected candidates. **a** colour-magnitude diagram for 117 known stars and 50 new YSO candidates. **b** colour-colour diagram for 115 known stars and 34 new YSO candidates. The main sequence (**a** and **b**), the giants branch **b** and the extinction vector are also plotted

(Feigelson & Kriss, 1989; Schwartz, 1991; Prusti et al., 1991; Gauvin & Strom, 1992; Hartigan, 1993; Lawson et al., 1996) and the DENIS candidates. The magnitudes given for the known T Tauri Stars (TTS) come from the DENIS observations.

The known TTS consists of Classical and Weak-line TTS (Feigelson et al., 1993). The weak-line or naked (Feigelson & Kriss, 1989) TTS show only little infrared excess and they are characterised by a $EW(H_\alpha) < 10$ Å. It corresponds to a later stage of evolution when a large fraction of the circumstellar material has been accreted. Hence, our candidates are likely to be classical TTS with strong emission lines and massive circumstellar accretion disks. We stress the point that our estimation of reddening is an upper limit. This explains that already known TTS are represented on the left of the main sequence in the colour-magnitude diagram and in the lower left corner of the colour-colour diagram. These objects probably lie on the front side of the cloud and thus do not suffer the total extinction that we have derived on the line of sight.

The brightest candidates are represented in an area of the diagram where already known TTS are found. Most of the known TTS have a smaller value of $J - K_\mathrm{s}$, but if we try to extend our sample toward bluer colours, we would enter an area corresponding to the giant and sub-giant stars, where no separation can reliably be made on the basis of near-IR colours.

Moreover, very few known TTS are as red as the DENIS candidates. An explanation could be an underestimation of the dereddening, but the colour-colour diagram indicates that at least 13 objects (detected in the 3 colours) cannot be shifted toward the main sequence simply by removing an additional reddening component. These candidates are among the reddest objects detected by DENIS. They were not previously detected because they are too faint and/or too far away of the cores. The cross-identification of DENIS and ROSAT pointed observations in the Cha I (Feigelson et al., 1993) shows that all X-ray sources detected by ROSAT are brighter than $K_\mathrm{s} \simeq 11$ and they do not exhibit strong infrared excess.

The spatial distribution of the candidates (Fig. 3) is also very remarkable. These sources have a trend to be concentrated near the cores of the cloud which strongly argue in favour of their young nature, since background giant stars would be uniformly spread over the whole field. Another interpretation remains: we could be in presence of small dark clumps that were not resolved in our extinction map. Then, an additional reddening would have to be taken into account, but, again, only a fraction of the candidate locations in colour–colour diagrams can be explained by normal reddening. In such case, the clumps should be smaller than $2'$ and would produce a visual extinction greater than 15 magnitudes. Although this interpretation cannot be definitely ruled out, we assume that these objects are more likely to be true young TTS, since the high infrared excess probably reveals the presence of a large amount of circumstellar material.

Finally, we have examined the interpretation that some of these stars could be brown dwarfs. On the theoretical evolutionary tracks for low–mass stars, young brown dwarfs are actually about 3 magnitudes brighter in K than old ones, hence, they could be detected at the distance of Cha I at our sensitivity limit. Comerón et al. (1998) have, indeed, reported the possible discovery of brown dwarfs in the ρ Oph molecular cloud at a comparable distance of 160 pc. However, the $J - K$ excess of young brown dwarfs is generally smaller than 1.5 and the $I - J$ is greater than 3.5. Since our faintest candidates have all $J - K > 2$ and $I - J < 2$, we conclude that they are unlikely to be brown dwarfs.

4.2. Evolutionary status of the new candidates

In order to evaluate the stage of evolution of these new objects, we have attempted to compare their position in a HR diagram with the evolutionary tracks modelled by D'Antona & Mazzitelli (1994). Since this model does not take into account the circumstellar contribution, it is necessary to evaluate the respective contributions of the stellar and circumstellar compo-

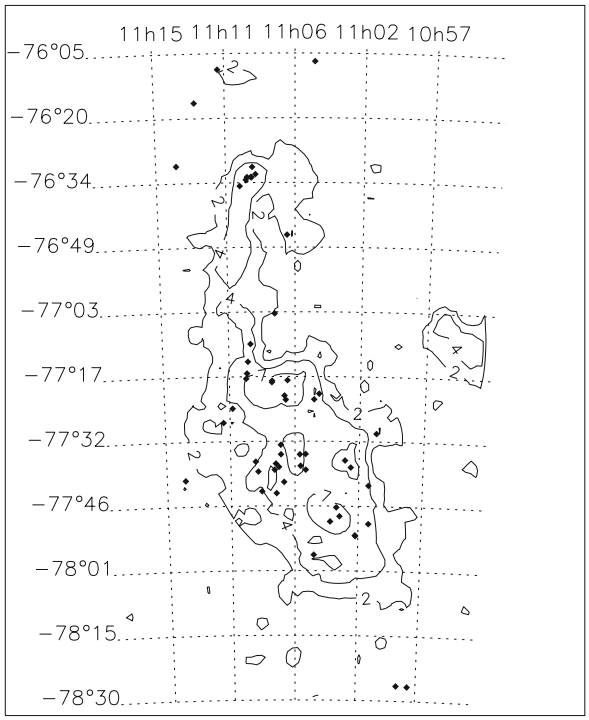

Fig. 3. Spatial distribution of YSOs candidates. Extinction isocontour at 2,4 and 7 A_V are also plotted

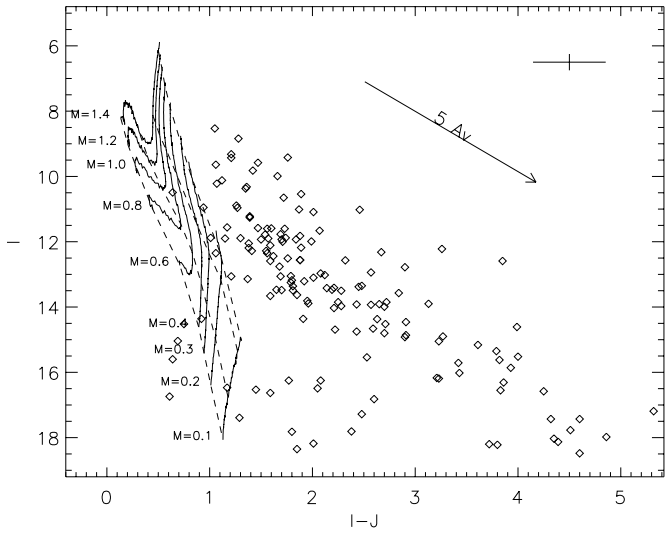

Fig. 4. Representation of the associated members of the cloud in a colour-magnitude diagram with pre-main-sequence tracks derived from the model of D'Antona & Mazzitelli (1994). Dashed lines are the isochrones at 10^5, 10^6, 10^7 and 10^8 years

nents to the emergent flux. The TTS, especially the classical ones are surrounded by massive circumstellar accretion disks which produces both extinction and emission. The extinction is caused by the dust grains, but the emission process is more intricate. Rydgren & Zak (1987) have shown that the infrared excess cannot be explained only in terms of thermal emission of grains in the circumstellar disk. An intrinsic disk luminosity contribution is required to account for the observations. They have shown that the intensity of the intrinsic component is directly related to the accretion rate and has the same order of magnitude as the thermal emission. According to Calvet et al. (1997) the near-infrared emission of protostars is largely dominated by an infalling dusty envelope emission. Protostars correspond to Class I objects (Lada, 1987; André & Montmerle, 1994) with massive envelopes. TTS are Class II or Class III objects, the essential of their circumstellar matter is in the accretion disk. Meyer et al. (1997) suggest that the infrared excess of TTS is essentially due to the disk emission, without any envelope effect. They found accretion rates in the range from 10^{-8} to $10^{-6} M_{\odot}.\mathrm{yr}^{-1}$ and inner disk radii from 2 to 6 R_*.

Fortunately, the contribution of the disk to the emission is likely to be negligible at wavelengths shorter than $\sim 1.6\ \mu\mathrm{m}$. Then, the I, and, with probably less confidence, the J fluxes can be considered as mainly of photospheric origin, although assuming no I excess, Meyer et al. (1997) have estimated the J excess to be only 10% of the photospheric flux for the classical TTS and to 0 for weak–line TTS. Thus, the colour excess is a good estimator of the extinction suffered by the star. The use of the $I-J$ colour excess may lead to underestimating the extinction because of the intrinsic luminosity of the accretion disc, but probably not more than 50%.

In order to convert the evolutionary tracks in the HR diagram of D'Antona & Mazzitelli (1994) into similar tracks in colour–magnitude diagram we use the Flower's table (1996) which gives the bolometric correction for the V band versus the effective temperature. Assuming that the star photosphere emits like a black body at the effective temperature, we derive V, I and J. The comparison of the main–sequence that we have constructed in this way with main–sequences based upon observations by Bessel & Brett (1988) and Johnson (1966) indicates that the assumption that the photosphere radiates like a black body is basically correct for these colours. We remark that it is not the case for the G4-M6 spectral range in the K_{s} band.

Previous studies have shown that the associated members of the Cha I cloud are essentially in the K7-M5 spectral range (Appenzeller et al., 1983; Lawson et al., 1996). Assuming that all stars are of spectral type M0 we can estimate the extinction they suffer. Fig. 4 shows a $I-J$ versus I diagram where all the TTS (known and candidates) are represented. The representation of the stars is clearly distributed along the reddening vector. Their position is compatible with a M0 spectral type ($M \simeq 0.6 M_{\odot}$) except for a part of the faintest sources for which $M \lesssim 0.2 M_{\odot}$ seems to be more appropriate. Note that 22 stars are missing because they are not detected in I. The extinction values that we have taken for each individual source are given in Tables 1 and 2. The restriction to the M0 spectral type implies uncertainties smaller than 1 magnitude of visual extinction because the tracks for different masses remain very close to each other.

Without a circumstellar component, we should have $A_V(star) \leq A_V(cloud)$ – the equality standing for a star just located behind the cloud. In Fig. 5 we remark that less

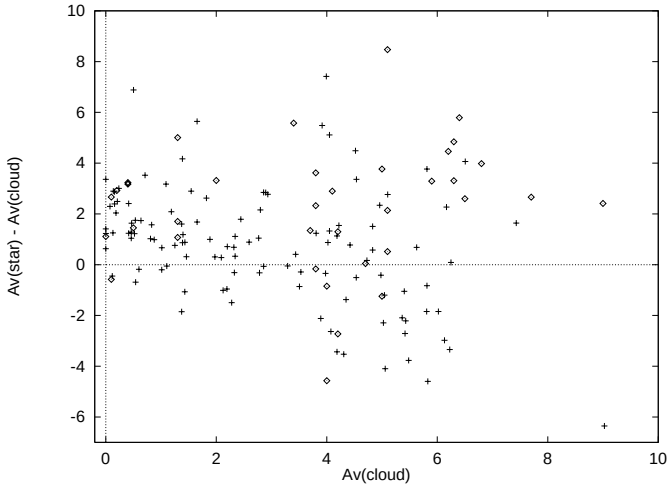

Fig. 5. Difference between extinction estimated from star count (cloud extinction) and from $I-J$ colour excess versus cloud extinction. Diamonds represent the DENIS candidates and crosses the known TTS

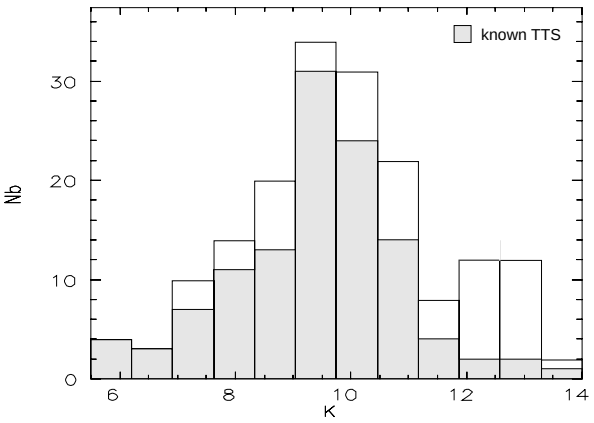

Fig. 6. The $K_{\rm s}$ Luminosity Function (KLF) for the associated members of the cloud. The previously known TTS are represented in grey

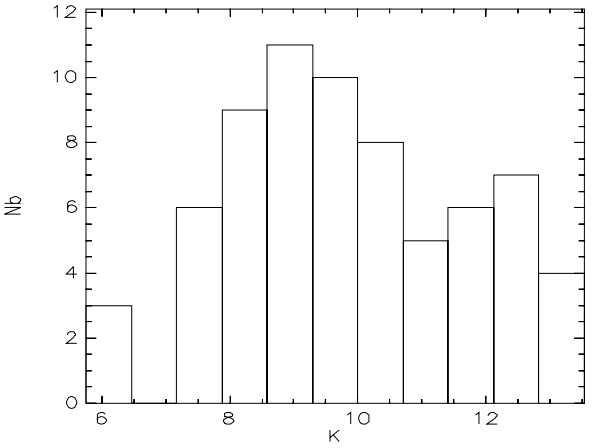

Fig. 7. The $K_{\rm s}$ Luminosity Function (KLF) for the DENIS selected members of the cloud (new candidates and the 16 reddest known TTS)

than $1/3$ of the stars are in that case. The dispersion of $A_V(star) - A_V(cloud)$ increases with $A_V(cloud)$. A first explanation could be simply the fact that the location of each star within the cloud is not known precisely. Moreover, the separation between circumstellar and cloud extinction is not possible. Another explanation could be the evolutionary stage of the star, the closer a star is to its forming area (i.e. the most obscured regions) the younger it is likely to be. So, this dispersion may result from the effect of the circumstellar disk properties : mass, inclination. Fig. 5 shows that visual extinction for stars is smaller than 10 magnitudes which confirms they are likely to be TTS rather than protostars (Lada & Adams, 1992). Protostars have massive envelopes which cause greater extinction of up to tens of magnitudes. Nevertheless, only stars detected in I are represented and, among the 6 stars detected only in $K_{\rm s}$, 4 are also detected by ISO (IRS4 and IRS5 in Table 1; nb 23 and 41 in Table 2) in the LW2 and LW3 filters centred at $6.75\ \mu$m and $15.0\ \mu$m, respectively (P. Persi, private communication). These sources are thus likely to be protostars of Class I. According to Prusti et al (1991) Ced110 IRS4 and IRS6 are confirmed Class I objects.

4.3. The luminosity function

Based on a study of the solar neighbourhood stellar population, Miller & Scalo (1979) have derived the IMF from the V luminosity function of main-sequence stars, and concluded that the IMF can be well approximated by a half-Gaussian distribution. In star-forming regions the population consists of YSOs often too faint in V or too highly reddened to be seen on Schmidt plates. The K band is the most appropriate to investigate the luminosity function in these areas (Lada et al., 1993; Megeath, 1996; Giovannetti et al., 1998). Fig. 6 displays the $K_{\rm s}$ luminosity function (KLF) for the TTS of the cloud including known sources and our candidates. The sample of known stars merge various observations that may be neither homogeneous, nor complete, since stars have been selected according to various criteria: Hα emission, near-infrared excess or X-ray emission. Examination of the KLF (Fig. 7) for all the DENIS selected objects shows 2 turnovers, the first one at $K_{\rm s} \simeq 9.5$ in the KLF is probably real while the second one at $K_{\rm s} \simeq 12.5$ corresponds to the DENIS completeness limit.

The interpretation of the luminosity function requires a model for the star formation. Theoretical evolutionary tracks (D'Antona & Mazzitelli, 1994) are used to derive a mass-luminosity relation. Stellar $K_{\rm s}$ magnitudes are computed assuming that they radiate like a black-body at their effective temperature and are calibrated using the standard solar parameters. We compute the mass-luminosity relation for 44 ages ranging from 10^5 to 10^8 years. We obtain similar results as Zinnecker & McCaughrean (1991) who have derived the relation for the ages $3\,10^5$, $7\,10^5$, 10^6, $2\,10^6$ years. To estimate when the star formation occurs in the cloud, we use the half-Gaussian IMF given by Miller & Scalo (1979). A Monte-Carlo simulation gives the 44 luminosity functions $\phi_i(K_{\rm s})$ for each age corresponding to a mass-luminosity relation. Since each theoretical KLF, $\phi_i(K_{\rm s})$, corresponds to a given age, the observed DENIS KLF can be fitted by a sum of $\phi_i(K_{\rm s})$ with different weight coefficients a_i.

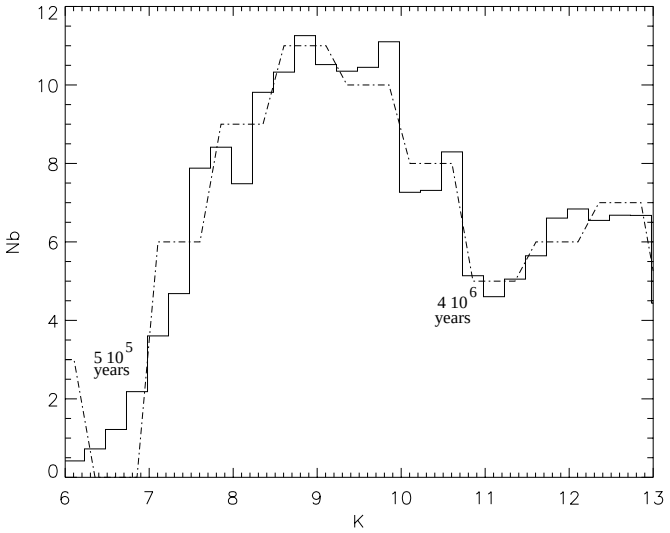

Fig. 8. The DENIS KLF (dashed line) and the simulated KLF (solid line)

The solution consists in the resolution of the linear system of equations :

$$\sum_{i=10^5 yr}^{10^8 yr} a_i \times \phi_i(K_\mathrm{s}) = \Phi(K_\mathrm{s})$$

The singular value decomposition is used to invert the matrix and then, derive the a_i coefficients. When a coefficient is found to be negative, the corresponding luminosity function is removed and the process is iterated with the remaining luminosity functions. Fig. 8 shows the simulated KLF and the DENIS KLF. Because of the small number of stars, the birth rate function cannot be derived accurately. The Poissonian errors do not allow the determination of its shape (increasing, constant or decreasing with time).

Nevertheless, the presence of two peaks in the KLF allows the estimate of the age of the sample. At first glance, one could invoke another period of star formation to explain the second peak at $K_\mathrm{s} \simeq 12.5$. This interpretation would, however, require stars older than $3\,10^7$ years which is in contradiction with our criterion that selects only stars with massive circumstellar accretion disks. Since the accretion rate is known to be about $10^{-7} M_\odot.\mathrm{yr}^{-1}$ (Meyer et al., 1997) our selected stars cannot be older than a few million years and this interpretation should be ruled out.

To explain this peak, several factors should be taken into account. The intrinsic dispersion of the magnitudes and the completeness limit imply a Malmquist bias which causes an overestimation of the number of faintest stars. This bias is about $5\,10^{-3}$ magnitude and so, can be ignored. Examination of the position of the 9 stars fainter than $K_\mathrm{s} = 11$ and detected in the three colours (9 objects) in a colour-colour diagram shows that their extreme colour cannot be interpreted in terms of reddening, hence high extinction clumps on their line of sight cannot be invoked.

Among the 11 stars which are not detected in I, 3 (nb 36, 43 and 44) lie in the direction of the molecular outflow observed in CO lines by Mattila et al. (1989) in a 22″ beam size. In this direction, they estimate a visual extinction of 17 magnitudes. Since our estimate of the extinction in this area is only 6 magnitudes with a 2′ resolution map, these stars can be background objects.

The 6 stars detected only in K_s also contribute to the second peak. Some of them are known protostars (IRS4 and IRS6 in Table 1) and others are likely to be so (see above). Their faintness results from the effect of a massive circumstellar envelope. We remark that the star responsible for the outflow cited above could be the star nb 41, detected only in K_s, rather than the known source T42 = sz32 (Persi P., private communication). Finally, possible unresolved binaries would lead to misleading colours that cannot be corrected. So, this peak is not fully understood and further deeper observations in K are requested to reach a better completeness limit.

The first peak at $K_\mathrm{s} \simeq 9$ requires a period of star formation that would extend from $4\,10^5$ to $3\,10^6$ years. Besides, the K_s excess modifies the luminosity function with a mean of 1.5 magnitude with respect to the spectral energy distribution of a main–sequence star. The mean extinction suffered by stars is about 5 magnitudes of visual extinction (Fig. 5), i.e. 0.5 magnitude of K_s extinction. The combination of these two effects shifts the KLF of 1 magnitude toward the fainter magnitudes. That led us to change our age estimation from $4\,10^5 - 3\,10^6$ to $5\,10^5 - 4\,10^6$ years. We stress the point that it just means that we do not detect older stars with our infrared excess criterion. Older stars have lost their disk, or, the accretion rate has become smaller and then, they no longer exhibit an infrared excess. The apparent drop of the KLF down to $K \simeq 11$ probably results from a vanishing of the circumstellar disk rather than from a real decrease of the star formation rate. The maximum life time of a circumstellar disk is then estimated to $4\,10^6$ years for low-mass stars which corresponds to the oldest Classical TTS.

5. Conclusion

The investigation of the DENIS data obtained in the Cha I cloud allowed the identification of 54 new faint YSOs candidates. They are selected on the basis of a large infrared excess and their concentration near to the cores of the cloud. Because of their IR excess they are likely to be surrounded by a massive circumstellar disk for which the visual extinction can reach 10 magnitudes (Fig. 5) and thus are probably Classical TTS. Comparison of the different magnitudes in the three DENIS channels shows that the K_s excess is ~ 1.5 magnitudes, in agreement with Meyer et al. (1997) who estimate from spectroscopic observations a K excess smaller than 1.6 magnitudes. Investigations on the K_s Luminosity Function down to $K_\mathrm{s} = 13$ shows important results concerning the age of our sample. First of all, youngest stars in the Cha I cloud are about $5\,10^5$ years, except for few protostars. Moreover, the decrease of the KLF for $K_\mathrm{s} > 10$ indicates that stars older than $4\,10^6$ years have

lost their circumstellar disk. The maximum life time of active disk is estimated to $4\,10^6$ years, after this period, the accretion becomes too small ($< 10^{-8} M_{\odot}.\mathrm{yr}^{-1}$) to produce an infrared excess. Spectroscopic follow-up of this new sample is underway to confirm definitely the nature of the newly discovered objects.

Acknowledgements. The DENIS team is warmly thanked for making this work possible and in particular the operations team at La Silla. The DENIS project is supported by the European Southern Observatory, in France by the *Institut National des Sciences de l'Univers*, the Education Ministry and the *Centre National de la Recherche Scientifique*, in Germany by the State of Baden-Wurttemberg, in Spain by the DGICYT, in Italy by the Consiglio Nazionale delle Ricerche, in Austria by the Science Fund and Federal Ministry of Science, Transport and the Arts, in Brazil by the Foundation for the development of Scientific Research of the State of São Paulo (FAPESP), and formerly by the *SCIENCE* and the *Human Capital and Mobility* plans of the European Commission.

References

Assendorp R., Wesselius P., Prusti T., et al., 1990, MNRAS 247, 624
Alcalá J.M., Krautter J., Covino E., et al., 1997, A&A 319, 184
André P., Montmerle T., 1994, ApJ 420, 837
Appenzeller I., Mundt R., 1989, A&AR 1, 291
Appenzeller I., Krautter J., Jankovics I., 1983, A&AS 53, 291
Baud B., Beintema D., Wesselius P., et al., 1984, ApJ 278, L53
Bessell M., Brett J., 1988, PASP 100, 1134
Calvet N., Hartmann L., Strom S., 1997, ApJ 481, 912
Cambrésy L., Epchtein N., Copet E., et al., 1997, A&A 324, L5
Comerón F., Rieke G.H., Claes P., et al., 1998, A&A 335, 522
Copet E., Epchtein N., Rouan D., et al., 1998, A&A in press
D'Antona F., Mazzitelli I., 1994, ApJS 90, 467
Epchtein N., 1997, in: F. Garzón, N. Epchtein, A. Omont, B. Burton, P. Persi (eds.), The Impact of Large Scale Near–Infrared Sky Surveys, 15, Kluwer Academic Publishers, Tenerife
Feigelson E., Casanova S., Montmerle T., et al., 1993, ApJ 416, 623
Feigelson E., Kriss G., 1989, ApJ 338, 262
Flower P., 1996, ApJ 469, 355
Gauvin L., Strom K., 1992, ApJ 385, 217
Giovannetti P., Caux E., Nadeau D., et al., 1998, A&A 330, 990
Hartigan P., 1993, AJ 105, 1511
Henning T., Pfau W., Zinnecker H., et al., 1993, A&A 276, 129
Hyland A., Jones T., Mitchell R., 1982, MNRAS 201, 1095
Johnson H., 1966, ARA&A 4, 193
Jones T., Hyland A., Harvey P., et al., 1985, AJ 90, 1191
Lada C., 1987, in: M. Peimbert, J. Jugaku (eds.), Star Forming Regions , 1–18, IAU Symp. 115 , Kluwer
Lada C., Adams F., 1992, ApJ 393, 278
Lada C., Young E., Greene T., 1993, ApJ 408, 471
Lawson W., Feigelson E., Huenemoerder D., 1996, MNRAS 280, 1071
Mattila K., Liljeström T., Toriseva M., 1989, in: Low Mass Star Form. & Pre-Main sequence Objects , 153, ESO Workshop
Megeath S., 1996, A&A 311, 135
Meyer M., Calvet N., Hillenbrand L., 1997, AJ 114, 288
Miller G., Scalo J., 1979, ApJS 41, 513
Nordh L., Olofsson G., Abergel A., et al., 1996, A&A 315, L185
Prusti T., Clark F., Whittet D., et al., 1991, MNRAS 251, 303
Prusti T., Whittet D., Wesselius P., 1992, MNRAS 254, 361
Robin A., Crézé M., 1986, A&A 157, 71
Rydgren A., 1980, AJ 85, 444
Rydgren A., Zak D., 1987, PASP 99, 141
Schwartz R., 1977, ApJS 35,161
Schwartz R., 1991, in: B. Reipurth (ed.), Scientific Report, no. 11, 93, ESO
Whittet D., Kirrane T., Kilkenny D., et al., 1987, MNRAS 224, 497
Whittet D., Prusti T., Wesselius P., 1991, MNRAS 249, 319
Zinnecker H., McCaughrean M., 1991, in: Vulcano Workshop on Young Star Clusters and Early Stellar Evolution , vol. 62, 761–766, Societa Astronomica Italiana, Memorie